

11. M.C. Tang, R.W. Ziolkowski, and S. Xiao, Compact wideband printed flower-slot antenna, *Microwave Opt Technol Lett* 56 (2014), 1465–1468.
12. M. Naser-Moghadasi, A.R. Sadeghzadeh, R.K.M. Lou, et al. Semi fractal three leaf clovar-shaped CPW antenna for triple band operation, *Int J RF Microwave Compu Aided Eng* 25 (2015), 413–418.
13. S.R. Patre and S.P. Singh, Study of CPW-fed flower-shaped patch antenna for broadband applications, *Microwave Opt Technol Lett* 57 (2015), 2908–2913.
14. Ansys HFSS, Ansoft, Pittsburgh, PA [Online]. Available at: <http://www.ansys.com>
15. D.T. Nguyen, D.H. Lee, and H.C. Park, Very compact printed triple band-notched UWB antenna with quarter-wavelength slots, *IEEE Antennas Wireless Propag Lett* 11 (2012), 411–414.
16. M.M. Fakharian and P. Rezaei, Very compact palmate leaf-shaped CPW-fed monopole antenna for UWB applications, *Microwave Opt Technol Lett* 7 (2014), 1612–1616.

© 2016 Wiley Periodicals, Inc.

FOUR LTE LOW-BAND SMARTPHONE ANTENNAS AND THEIR MIMO PERFORMANCE WITH USER'S HAND PRESENCE

Kin-Lu Wong,¹ Yu-Chen Chen,¹ and Wei-Yu Li²

¹Department of Electrical Engineering, National Sun Yat-Sen University, Kaohsiung 80424, Taiwan; Corresponding author: wongkl@ema.ee.nsysu.edu.tw

²Information and Communications Research Laboratories Industrial Technology Research Institute, Hsinchu 31040, Taiwan

Received 21 January 2016

ABSTRACT: Owing to the narrow regions along the four edges of the modern smartphone, especially the two narrow regions along the long (side) edges thereof, it has been a design challenge to embed the internal antennas therein. The design challenge is especially critical for embedding the long-term evolution (LTE) low-band antennas with operating frequencies below 1 GHz. In this study, based on the open-slot antenna structure, the design of four LTE low-band antennas, respectively, disposed along the four edges of the smartphone are presented. The two antennas along the two short (top and bottom) edges have a low profile of 10 mm and can cover 698–960 MHz. The two antennas along the two long edges have a low profile of 1 mm only and can cover 824–960 MHz. The four antennas can be applied in a 4×4 multiple-input multiple-output (MIMO) system in the 824–960 MHz band (e.g., the LTE band 5 and 8). Conversely, the two short-edge antennas can be used for 2×2 MIMO in the 698–960 MHz band (e.g., the LTE band 5, 8, 13, and 17). The operating principle and antenna performance of the four antennas are presented. The obtained channel capacities for 4×4 MIMO and 2×2 MIMO operations are also shown. Effects of the user's hand holding the smartphone with the four antennas therein are also analyzed. © 2016 Wiley Periodicals, Inc. *Microwave Opt Technol Lett* 58:2046–2052, 2016; View this article online at wileyonlinelibrary.com. DOI 10.1002/mop.29969

Key words: mobile antennas; smartphone antennas; LTE antennas; MIMO operation; open-slot antennas; user's hand effects

1. INTRODUCTION

For the 2×2 multiple-input multiple-output (MIMO) operation to achieve enhanced channel capacity, two long-term evolution (LTE) antennas are required to be embedded in the smartphone [1–4]. It is also expected that the 4×4 MIMO operation can provide much higher channel capacity than the 2×2 MIMO operation [5]. However, owing to the very limited space avail-

able in the smartphone for the internal antennas therein, it has been a design challenge to embed more than two LTE antennas therein, especially for those with frequencies below 1 GHz. To the best of the authors' knowledge, it is noted that the design of four LTE smartphone antennas that can cover the LTE low band below 1 GHz is still not reported in the open literature.

In this article, the design of four LTE low-band antennas in the smartphone for the 4×4 MIMO system is presented. The four antennas are based on the open-slot antenna structure [6,7] to operate in the LTE low band and are, respectively, disposed along the four edges of the smartphone. The two antennas along the two short (top and bottom) edges of the smartphone can cover 698–960 MHz and have a low profile of 10 mm to the short edges thereof. Conversely, the two antennas along the two long (side) edges can cover 824–960 MHz and have a low profile of 1 mm to the long edges thereof. The 1-mm low profile makes it promising to be applied in the modern smartphone with a large display panel therein. In addition, the four LTE low-band antennas in the proposed design also show good envelope correlation coefficients (ECCs) [8,9] (less than about 0.2 in 824–960 MHz) between any two antennas thereof. This makes it attractive for practical applications.

In this study, the operating principle and antenna performance, including the MIMO performance (ECCs and channel capacities), of the four antennas are presented. The four antennas (two short-edge and two long-edge antennas together) can be applied in a 4×4 MIMO system in the 824–960 MHz band, which, for example, covers the LTE band 5 and 8 [10]. Conversely, the two short-edge antennas alone can be used for the 2×2 MIMO operation in the 698–960 MHz band, which for example covers the LTE band 5, 8, 13, and 17 [10]. Effects of the user's hand holding the smartphone in the one-hand and two-hand data modes with the four antennas therein for the MIMO operation are also analyzed.

2. FOUR LTE LOW-BAND MIMO ANTENNAS

2.1. Structure of the Four Antennas (Ant1, Ant2, Ant3, Ant4)

Figure 1 shows the geometry of four LTE low-band antennas, respectively, disposed along four edges of the main circuit board in the smartphone. The main circuit board is selected to have dimensions of 75×150 mm². The dielectric frame of width 6 mm with metallic plate printed on the inner surface thereof is attached around the four edges of the main circuit board. The metallic plate thereon is also connected to the system ground plane printed on the back side of the main circuit board. Both the main circuit board and dielectric frame are fabricated using 0.8-mm thick FR4 substrate of relative permittivity 4.4 and loss tangent 0.02. The smartphone based on the structure has a total size of $76.6 \times 151.6 \times 6$ mm³, which is reasonable for the modern smartphones on the market.

The four antennas are all based on the open-slot antenna structure. They include two short-edge (SE) antennas along the short edges thereof and two long-edge (LE) antennas along the long edges thereof. The two SE antennas (Ant1 and Ant2) and two LE antennas (Ant3 and Ant4) all have simple and compact structures. Both Ant1 and Ant2 have same antenna structure, and Ant3 and Ant4 are also identical in their structures. Linear open slots of length 57 mm and width 2 mm are used for the SE antennas. Also note that, for either Ant1 or Ant2, there is a 2-mm gap at the opening of the linear open slot on the metallic plate of the long-edge frame. Ant1 and Ant2 also show a low profile of 10 mm to the top- or bottom-edge frame. To excite Ant1 or Ant2 to generate its quarter-wavelength slot mode with enhanced impedance matching [11], the microstrip feedline is

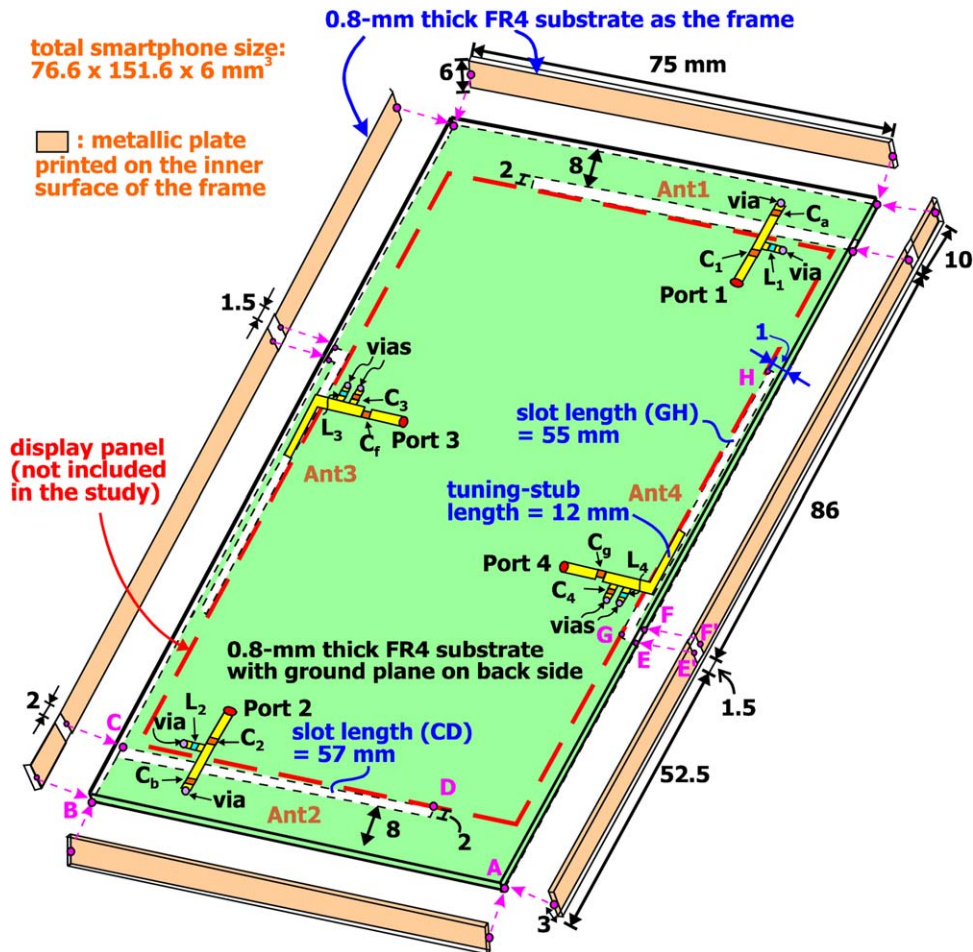


Figure 1 Geometry of four LTE low-band antennas disposed along four edges of the main circuit board in the smartphone. [Color figure can be viewed in the online issue, which is available at wileyonlinelibrary.com.]

shorted to the ground plane at its one end and embedded therein with a capacitor C_a or C_b (0.3 pF) and a high-pass matching circuit L_1 , C_1 or L_2 , C_2 (13 nH, 1.7 pF). Detailed dimensions and loaded circuit elements of Ant1 or Ant2 are shown in Figure 2. Ant1 and Ant2 can cover the 698–960 MHz band.

The two LE antennas (Ant3 and Ant4) use the inverted-L open slots of length 55 mm and width 0.5 mm. There is also a 1.5-mm gap at the long-edge frame at the opening of the open slot for Ant3 or Ant4. The detailed dimensions are shown in Figure 3. Note that Ant3 and Ant4 have a very low profile of 1 mm to the long-edge frame, which makes it promising to be

disposed in the narrow region between the display panel and the long-edge frame. The microstrip feedline uses an open-end tuning stub of length 12 mm, a band-pass matching circuit L_3 , C_3

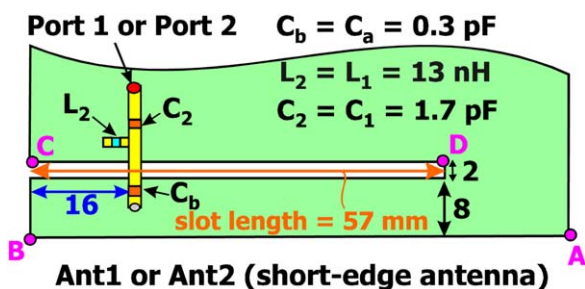


Figure 2 Dimensions of Ant1 or Ant2 along one short edge of the main circuit board. [Color figure can be viewed in the online issue, which is available at wileyonlinelibrary.com.]

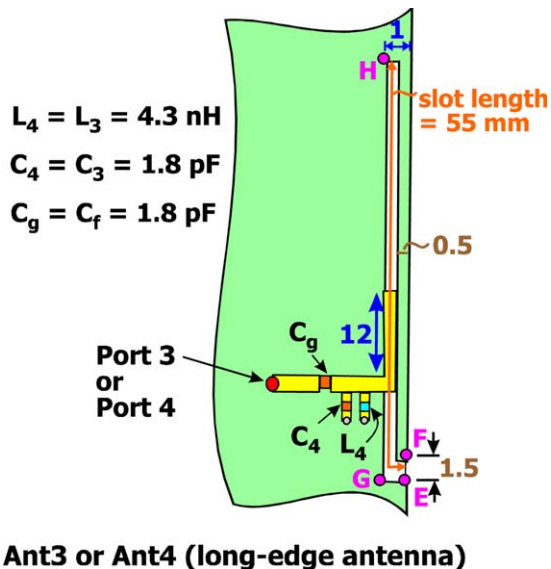


Figure 3 Dimensions of Ant3 or Ant4 along one long edge of the main circuit board. [Color figure can be viewed in the online issue, which is available at wileyonlinelibrary.com.]

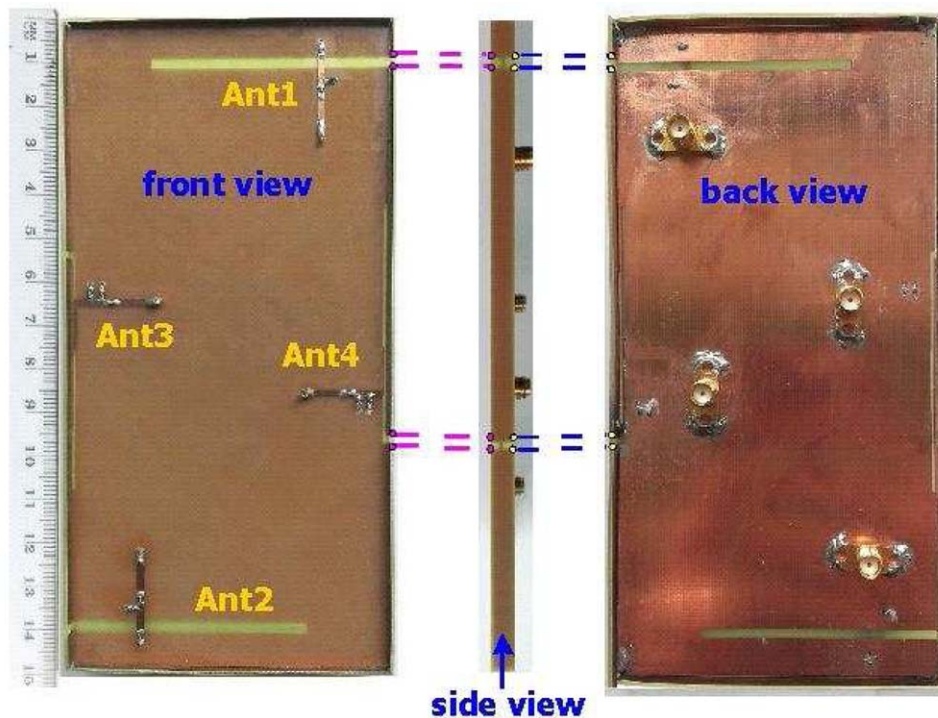


Figure 4 Photos of the fabricated antennas. [Color figure can be viewed in the online issue, which is available at wileyonlinelibrary.com.]

or L_4 , C_4 (4.3 nH, 1.8 pF), and a tuning capacitor C_f or C_g (1.8 pF). Using the microstrip feedline with the embedded circuit elements, the quarter-wavelength slot mode with enhanced impedance matching can be generated. Ant3 and Ant4 can cover 824–960 MHz. To provide a more clear description of the four antennas, the photos of the fabricated antennas are shown in Figure 4. The operating principle and antenna performance of Ant1 to Ant4 and their MIMO performances are presented in the following sections.

2.2. Operating Principle and Antenna Performance

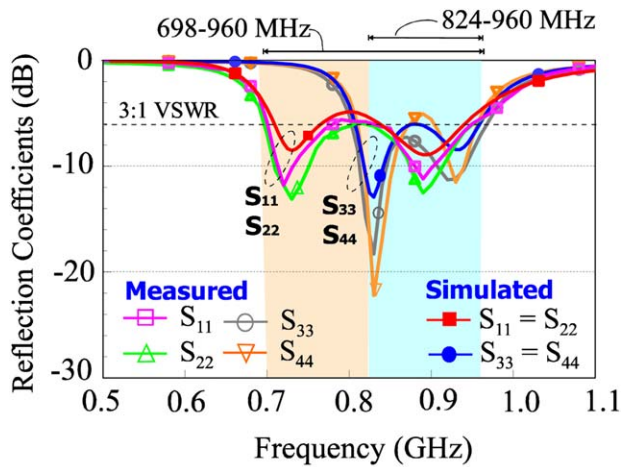
Figures 5(a) and 5(b) shows the measured and simulated S parameters (reflection and transmission coefficients) of the four antennas. The full-wave high frequency structure simulator HFSS version 16 [12] is applied in obtaining the simulated results. The measured data for the fabricated antenna shown in Figure 4 are also shown for comparison. The measurement and simulation are generally show good agreement. As shown in Figure 5(a), the measured reflection coefficients of Ant1 and Ant2 show acceptable impedance matching better than about -6 dB in 698–960 MHz (see S_{11} and S_{22} curve). Conversely, that of Ant3 and Ant4 can cover 824–960 MHz with an impedance matching better than about -6 dB (see S_{33} and S_{44} curve). From Figure 5(b), the obtained transmission coefficients indicate that the isolation of two SE antennas (Ant1 and Ant2, see S_{12} curve) is better than 10 dB and that of two LE antennas (Ant3 and Ant4, see S_{34} curve) is better than 15 dB. The isolation between one SE antenna and one LE antenna is also better than about 10 dB for Ant1 and Ant4 (see S_{14} curve) or better than about 14 dB for Ant1 and Ant3 (see S_{13} curve).

Figure 6 shows the measured and simulated antenna efficiencies for the four antennas. The measured antenna efficiencies are obtained in a far-field anechoic chamber. The result of Ant1 is measured with three other antennas terminated to 50- Ω loads.

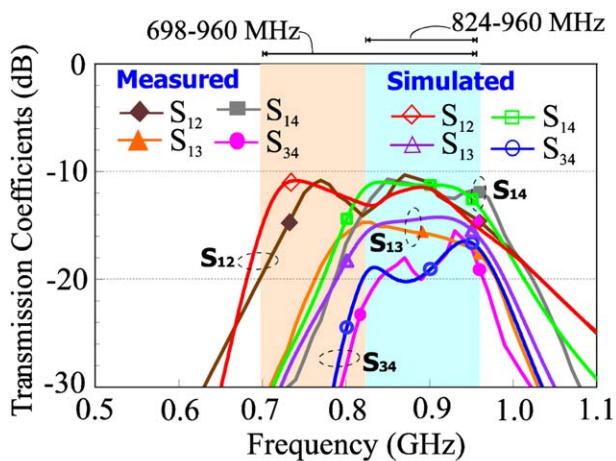
Those of Ant2 to Ant4 are measured similarly. From the results, agreement between the measurement and simulation is seen. The measured antenna efficiencies of Ant1 and Ant2 are also generally about the same and vary from about 40% to 52%. For Ant3 and Ant4, their measured antenna efficiencies are also similar and vary from about 30% to 37%. Note that, owing to the mutual coupling between the four antennas, the antenna efficiencies of Ant1 to Ant4 are decreased as compared to the case with only one or two antennas in operation. A comparison of the simulated antenna efficiencies for the cases with different numbers of the antennas in operation is presented in Figure 7.

In Figure 7, Case 1 shows the case of Ant1 in operation (ON) with other three antennas left open (OFF, not connected to 50- Ω loads). Case 2 is the case of Ant1 and Ant2 in operation (ON) with other two antennas left open (OFF). Case 3 is the case of Ant3 in operation (ON) with other three antennas left open (OFF), and Case 4 is the case of Ant1 and Ant3 in operation (ON) with other two antennas left open (OFF). For Case 1, Ant1 has an antenna efficiency of about 50% to 67%. When Ant2 is also in operation (that is, Case 2), the antenna efficiency of Ant1 is decreased to be about 47% to 58%, owing to the coupling between Ant1 and Ant2.

Conversely, when only Ant3 is in operation (Case 3), the antenna efficiency of Ant3 is about 47% to 58%. When only Ant3 and Ant1 are in operation, the antenna efficiency of Ant3 is about 34% to 50% and that of Ant1 is about 42% to 65%. The results in Figures 6 and 7 indicate that the coupling between the four antennas will decrease the antenna efficiency. However, the antenna efficiencies for Ant1 and Ant2 only (Case 2) are better than about 47%, which is acceptable for 2×2 LTE MIMO operation [13]. In addition, for all four antennas (Ant1 to Ant4) in operation (the case in Fig. 6), the simulated antenna efficiencies of Ant1 and Ant2 are still about 38% to 52% in 824–960 MHz, and those of Ant3 and Ant4 are about 30% to 37%. In this condition, the computed channel capacity



(a)



(b)

Figure 5 Measured and simulated (HFSS) (a) reflection coefficients and (b) transmission coefficients of the four antennas. [Color figure can be viewed in the online issue, which is available at wileyonlinelibrary.com.]

for 4×4 LTE MIMO operation reaches about 17 bps/Hz, much better than that for 2×2 LTE MIMO operation (see Fig. 11). The results will be discussed later in Section 2.4 with the aid of Figure 11.

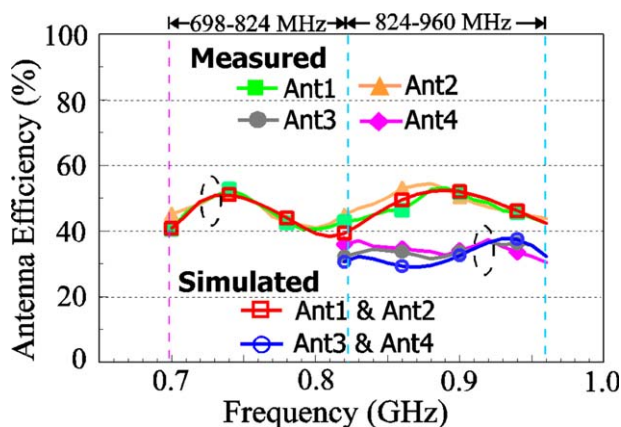
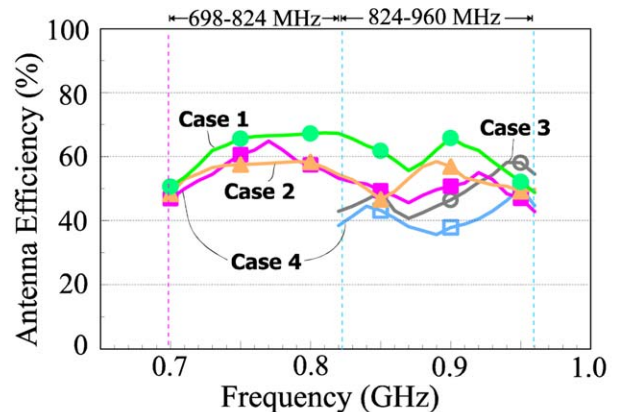


Figure 6 Measured and simulated (HFSS) antenna efficiencies for the four antennas. [Color figure can be viewed in the online issue, which is available at wileyonlinelibrary.com.]



Case 1 —●— Ant1 ON (Others OFF)
Case 2 —▲— Ant1 & Ant2 ON, Ant3 & Ant4 OFF
Case 3 —○— Ant3 ON (Others OFF)
Case 4 —■— Ant1 ON, Ant3 ON (Ant2 & Ant4 OFF)

Figure 7 Simulated (HFSS) antenna efficiencies for different numbers of the antennas in operation. Case 1: Ant1 ON with other three antennas OFF. Case 2: Ant1 and Ant2 ON with other two antennas OFF. Case 3: Ant3 ON with other three antennas OFF. Case 4: Ant1 and Ant3 ON with other two antennas OFF. [Color figure can be viewed in the online issue, which is available at wileyonlinelibrary.com.]

The measured three-dimensional total-power radiation patterns for the four antennas are also analyzed. Figure 8 shows the representative results at 0.89 MHz. It is seen that strong radiation for Ant1 is about in the $+y$ direction and that for Ant2 is about in the $-y$ direction. Conversely, Ant3 radiates strongly in the quadrant between the $+z$ and $-y$ axes, whereas Ant4 radiates strongly in the quadrant between the $-z$ and $+y$ axes. The radiation patterns are different for the four antennas, which suggests that the four antennas have independent radiation characteristics and can result in better envelope correlation coefficients (ECCs) between the antennas.

Since the excited surface currents on the system ground plane will dominate the antenna's radiation characteristics for frequencies less than 1 GHz, the simulated surface current distributions on the system ground plane at 0.89 GHz are also presented in Figure 9. The results for four cases of only one antenna excited with others terminated to $50\text{-}\Omega$ loads are presented. The arrow shown in each case indicates the resonant direction of the excited surface currents. For Ant1 and Ant2, their resonant direction is orthogonal to that of Ant3 and Ant4. This indicates that the polarization direction of the radiation fields of Ant1 and Ant2 is generally orthogonal to that of Ant3 and Ant4. This will also lead to enhanced ECCs between the two SE antennas (Ant1 and Ant2) and the two LE antennas (Ant3 and Ant4).

2.3. Envelope Correlation Coefficients

The ECC results of the four antennas are studied in this section. Figure 10 shows the simulated (HFSS) and computed ECCs. The computed ECCs are obtained using the measured electric-field patterns of the four antennas. The simulated ECCs are obtained from the HFSS simulation results. Agreement between the simulated and computed ECCs is seen. The ECC between Ant1 and Ant2 is less than about 0.3 in 698–960 MHz, which is good for 2×2 MIMO [3,14]. For 4×4 MIMO in 824–960 MHz, even better ECCs (less than about 0.2) for any two

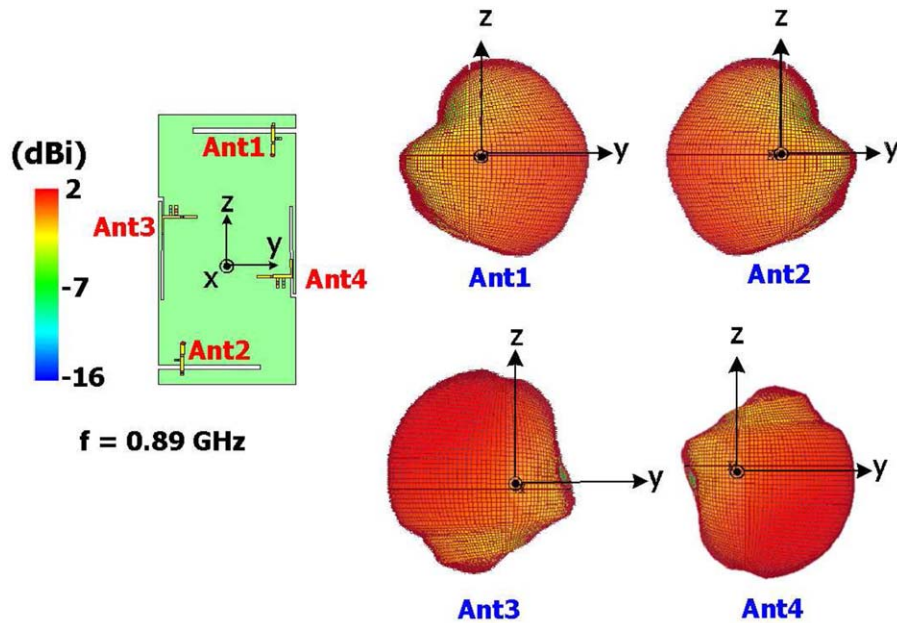


Figure 8 Measured three-dimensional total-power radiation patterns for the four antennas. [Color figure can be viewed in the online issue, which is available at wileyonlinelibrary.com.]

antennas therein are seen. This is in part owing to the orthogonal arrangement of the two SE antennas (Ant1 and Ant2) to the two LE antennas (Ant3 and Ant4), as discussed in Section 2.3.

2.4. Channel Capacities in a 4×4 MIMO System

Figure 11 shows the computed channel capacities from the HFSS simulated results and from the measured data of the four antennas for 4×4 MIMO in 824–960 MHz. The computed capacity from the HFSS simulated results of Ant1 and Ant2 for 2×2 MIMO in 698–960 MHz is also shown for comparison. The computed channel capacities are obtained by considering the Rayleigh fading propagation environment with identically and independently distributed (i.i.d.) channels [8,9]. The four antennas in the smartphone are for the receive antennas in the MIMO operation. For the transmit antennas, they are assumed to be uncorrelated and have perfect (100%) antenna efficiency. The computed channel capacities are obtained by averaging over 10,000 Rayleigh fading realizations with a signal-to-noise Ratio (SNR) of 20 dB. The results indicate that the channel capacity for 4×4 MIMO reaches about 17 bps/Hz, whereas that for 2×2 MIMO is about 9.5 bps/Hz. That is, the channel capacity of the four antennas (Ant1 to Ant4) in this study can have about 1.8 times that of two antennas (Ant1 and Ant2 only) for the MIMO operation. This also suggests that by including Ant3 and Ant4 for the MIMO operation, the channel capacity can increase by about 80%.

3. USER'S HAND EFFECTS

The case with the user's hand holding the smartphone is also studied. The results for analyzing the user's hand effects are obtained using the SEMCAD simulation [15]. The simulation models with the user's hand presence in the one-hand and two-hand data modes are shown in Figure 12. In Figure 12(a), the simulation model includes the four antennas (Ant1 to Ant4) for 4×4 MIMO. In Figure 12(b), only Ant1 and Ant2 are in the simulation model for 2×2 MIMO. Representative results of

the computed channel capacities at 860 MHz are listed in Table 1. The free space scenario considers that the user's hand is not present. In Table 1, the antenna efficiency (Eff) and ECC are also obtained using SEMCAD simulation for a fair comparison. Also, the ECC for 4×4 MIMO is the maximum value between any two antennas.

When there is no user's hand presence (free space scenario), the antenna efficiencies for Ant1 to Ant4 are 46%, 46%, 30%, and 30%, respectively. The antenna efficiencies for Ant1 and Ant2 for 2×2 MIMO are 54% and 54%, better than those for 4×4 MIMO. The ECCs (0.17 and 0.10) are also small and good for MIMO applications. In this scenario, the channel capacity for 4×4 MIMO reaches 16.90 bps/Hz at 20-dB SNR, about 1.8 times that (9.41 bps/Hz) for 2×2 MIMO.

For the one-hand data mode scenario, the antenna efficiencies decrease to 30%, 16%, 20%, and 10%. The relatively lower antenna efficiencies of Ant2 and Ant4 are mainly owing to the user's hand covering the antenna's open-slot opening. Similarly, for 2×2 MIMO, Ant2 also shows a lower antenna efficiency than Ant1 (15% vs. 18%). The ECCs in this scenario are also small (0.15 and 0.04) and the channel capacity for 4×4 MIMO can still be about 1.75 times that of 2×2 MIMO (13.30 vs. 7.62 bps/Hz).

For the two-hand data mode scenario, Ant2 shows smaller antenna efficiency than Ant1 (11% vs. 26% for 4×4 MIMO and 10% vs. 28% for 2×2 MIMO), also owing to the user's hand covering the antenna's open-slot opening. Because of the similar reason, Ant3 also shows smaller antenna efficiency than Ant4 (18% vs. 22%). The ECCs are also small in this case (0.12 and 0.02). It is interesting to note that the channel capacity for 4×4 MIMO is about 2.0 times that for 2×2 MIMO (13.30 vs. 7.62 bps/Hz). From the results in Table 1, it can be concluded that for both free space and user's hand presence, the channel capacity can be significantly increased by using the four antennas for 4×4 MIMO as compared to the use of Ant1 and Ant2 for 2×2 MIMO.

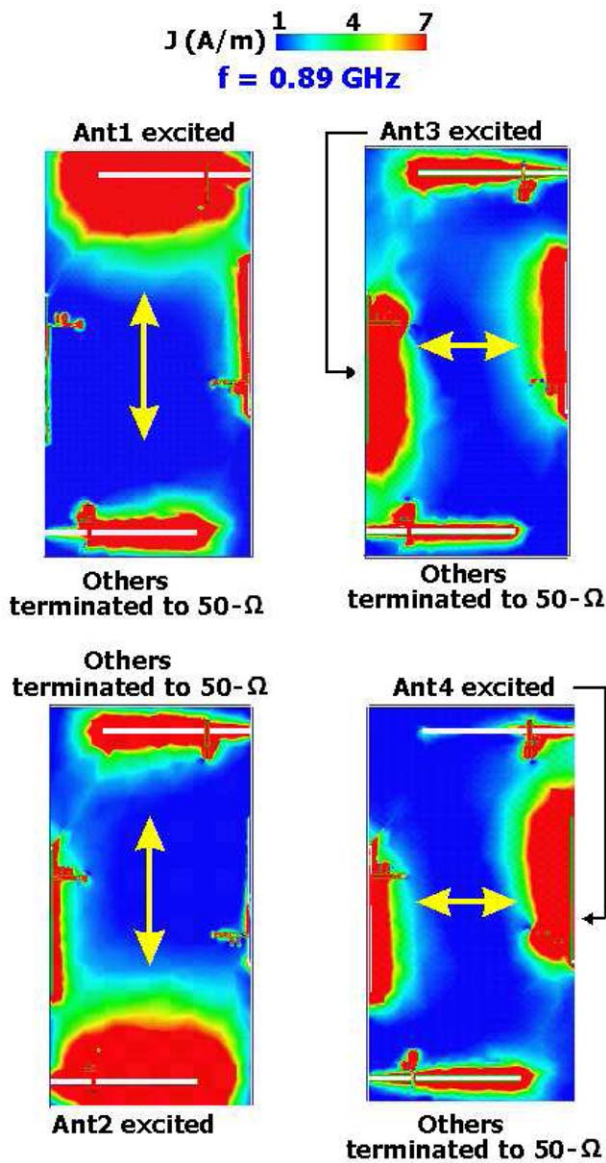


Figure 9 Simulated (HFSS) surface current distributions on the system ground plane for the four antennas. [Color figure can be viewed in the online issue, which is available at wileyonlinelibrary.com.]

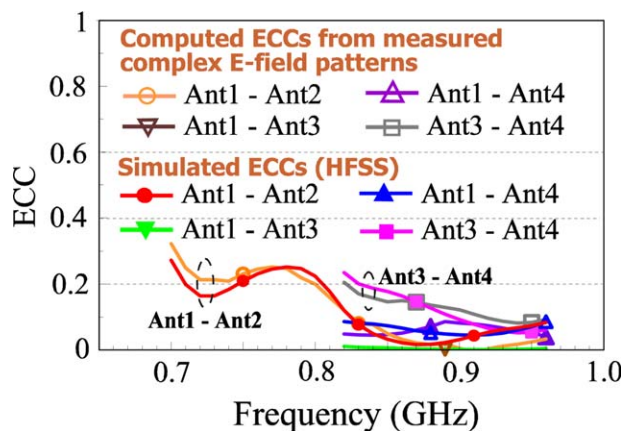


Figure 10 Simulated (HFSS) ECCs and computed ECCs from the measured electric-field patterns for the four antennas. [Color figure can be viewed in the online issue, which is available at wileyonlinelibrary.com.]

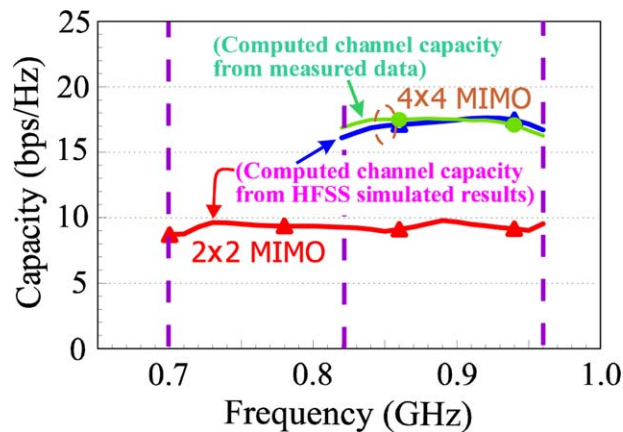


Figure 11 Computed channel capacities from the HFSS simulated results and from the measured data of the four antennas in a 4×4 MIMO system. [Color figure can be viewed in the online issue, which is available at wileyonlinelibrary.com.]

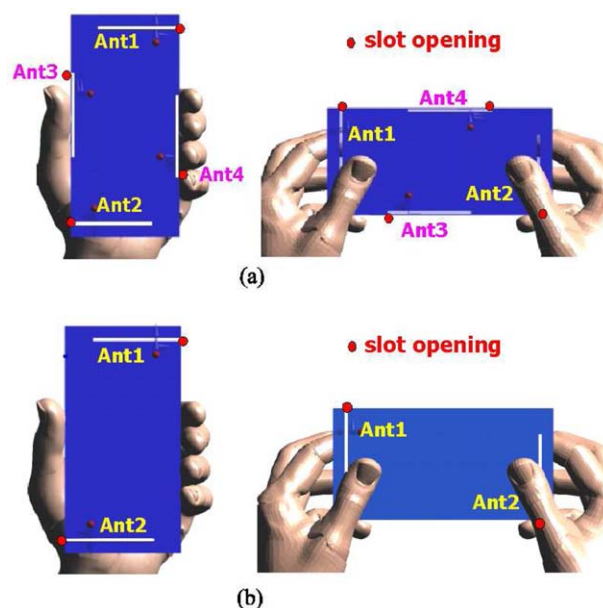


Figure 12 Simulation model (SEMCAD) for the case with user's hand presence. (a) Four antennas with one-hand and two-hand data modes. (b) Two antennas (Ant1 and Ant2 only, Ant3 and Ant4 not present) with one-hand and two-hand data modes. [Color figure can be viewed in the online issue, which is available at wileyonlinelibrary.com.]

4. CONCLUSION

The design of four LTE low-band antennas disposed in the smartphone to achieve good envelope correlation coefficients and enhanced channel capacity for the MIMO operation have been proposed. The four antennas are based on the open-slot antenna structure and show low profile (10 mm or 1 mm only) to the short edge and long edge, allowing a large display panel to be disposed in the smartphone. For free space case (no user's hand presence), the obtained channel capacities of the four antennas for 4×4 MIMO are found to be about 17 bps/Hz at 20-dB SNR in 824–960 MHz, about 1.8 times that for 2×2 MIMO. With the user's hand presence, the channel capacity for 4×4 MIMO is still much better than for 2×2 MIMO, especially for the two-hand data mode case. The obtained results in his study indicate that the four LTE low-band antennas are

TABLE 1 Computed Channel Capacities at 860 MHz for the Case With User's Hand Presence

Scenario		Ant1 Eff.	Ant2 Eff.	Ant3 Eff.	Ant4 Eff.	ECC	Capacity (bps/Hz)
Free space	4 × 4 MIMO	46%	46%	30%	30%	0.17	16.90
	2 × 2 MIMO	54%	54%	–	–	0.10	9.41
One-hand data mode	4 × 4 MIMO	30%	16%	20%	10%	0.15	13.30
	2 × 2 MIMO	35%	18%	–	–	0.04	7.62
Two-hand data mode	4 × 4 MIMO	26%	11%	18%	22%	0.12	13.40
	2 × 2 MIMO	28%	10%	–	–	0.02	6.65

The antenna efficiency (Eff) and ECC are obtained using SEMCAD with the simulation models shown in Figure 12. The ECC for 4 × 4 MIMO is the maximum value between any two antennas therein.

promising to be embedded in the modern smartphone and their MIMO performance is also good for practical applications.

REFERENCES

- H. Li, Z. Zachary, and B.K. Lau, Design of orthogonal MIMO handset antennas based on characteristic mode manipulation at frequency bands below 1 GHz, *IEEE Trans Antennas Propag* 62 (2014), 2756–2766.
- K.L. Wong, T.W. Kang, and M.F. Tu, Internal mobile phone antenna array for LTE/WWAN and LTE MIMO operations, *Microwave Opt Technol Lett* 53 (2011), 1569–1573.
- Y.L. Ban, S. Yang, Z. Chen, K. Kang, and J.L.W. Li, Decoupled planar WWAN antennas with T-shaped protruded ground for smartphone applications, *IEEE Antennas Wireless Propag* 13 (2014), 483–486.
- K.L. Wong, H.J. Jiang, and T.W. Weng, Small-size planar LTE/WWAN antenna and antenna array formed by the same for tablet computer application, *Microwave Opt Technol Lett* 55 (2013), 1928–1934.
- K. Werner, J. Furuskog, M. Riback, and B. Hagerman, Antenna configurations for 4 × 4 MIMO in LTE—Field measurement, In: *Proceedings of the 71st Vehicular Technology Conference (VTC 2010-Spring)*, Taipei, Taiwan, 2010, pp. 1–5.
- K.L. Wong and C.Y. Tsai, Low-profile dual-wideband inverted-T open slot antenna for the LTE/WWAN tablet computer with a metallic frame, *IEEE Trans Antennas Propag* 63 (2015), 2879–2886.
- C.I. Lin and K.L. Wong, Printed monopole slot antenna for internal multiband mobile phone antenna, *IEEE Trans Antennas Propag* 55 (2007), 3690–3697.
- K.L. Wong and J.Y. Lu, 3.6-GHz 10-antenna array for MIMO operation in the smartphone, *Microwave Opt Technol Lett* 57 (2015), 1699–1704.
- K.L. Wong, J.Y. Lu, L.Y. Chen, W.Y. Li, and Y.L. Ban, 8-antenna and 16-antenna arrays using the quad-antenna linear array as a building block for the 3.5-GHz LTE MIMO operation in the smartphone, *Microwave Opt Technol Lett* 58 (2016), 174–181.
- LTE Frequency Bands & Spectrum Allocations—a summary: Tables of the LTE frequency band spectrum allocations for 3G & 4G LTE. Available at: <http://www.radio-electronics.com/>
- K.L. Wong and P.R. Wu, Dual-wideband linear open slot antenna with two open ends for the LTE/WWAN smartphone, *Microwave Opt Technol Lett* 57 (2015), 1269–1274.
- ANSYS HFSS, Ansoft Corp., Pittsburgh, PA. Available at: <http://www.ansys.com/staticassets/ANSYS/staticassets/resourcelibrary/brochure/ansys-hfss-brochure-16.0.pdf>, 2015.
- K.L. Wong and M.T. Chen, Small-size LTE/WWAN printed loop antenna with an inductively coupled branch strip for bandwidth

enhancement in the tablet computer, *IEEE Trans Antennas Propag* 61 (2013), 6144–6151.

- M.S. Sharawi, Printed multi-band MIMO antenna systems and their performance metrics, *IEEE Antennas Propag Mag* 55 (2013), 218–232.
- SPEAG SEMCAD. Available at: <http://www.semcad.com>

© 2016 Wiley Periodicals, Inc.

A DUAL-BAND METAMATERIAL MICROWAVE ABSORBER

Jinpil Tak, Yunnan Jin, and Jaehoon Choi

Department of Electronics and Communications Engineering, Hanyang University, Seoul, Korea; Corresponding author: choijh@hanyang.ac.kr

Received 22 January 2016

ABSTRACT: A dual-band metamaterial microwave absorber for X band (8–12 GHz) applications is proposed. A unit cell of the absorber consists of an electric LC (ELC) resonator, a backing ground plate, and an FR4-epoxy substrate with 0.8 mm thickness. To realize efficient space utilization for the dual resonance, an ELC resonator consisting of asymmetric triangle split-ring resonators is adopted. Using effective medium parameters extracted from the S-parameters, the EM behavior is clarified to describe the operating mechanism. The miniaturized dimensions of the unit cell are 8 mm × 8 mm × 0.8 mm. The measured results exhibit two absorptivity peaks stronger than 98.5% and FWHMs of 8.4% and 7.25% at 8.2 GHz and 12 GHz, respectively. Additionally, high absorptivity performance is achieved for EM waves from 0° to 60° regardless of the incident angle. © 2016 Wiley Periodicals, Inc. *Microwave Opt Technol Lett* 58:2052–2057, 2016; View this article online at wileyonlinelibrary.com. DOI 10.1002/mop.29977

Key words: dual-band; metamaterial; microwave absorber; frequency selective surface

1. INTRODUCTION

Metamaterials (MTMs) are artificial electromagnetic structures periodically composed of metals and dielectrics. The initial MTM research addressed the realization of effective negative permittivity, permeability, and refractive indexes [1–5]. In particular, MTM thin electromagnetic wave absorbers have received a great deal of research attention due to their various potential applications, such as radar, concealment, and reduction of automotive false imaging. For example, a microwave absorber based on an MTM high-impedance surface that consisted of an array of split ring resonators (SRRs) spaced a distance above a ground plane and separated by a dielectric was proposed [6,7]. One solution for a thin MTM absorber is an electrical resonance-type absorber, called a frequency selective surface (FSS) absorber. Generally in FSS absorber design, a periodic resonator patch is located on the top side of a lossy substrate, and the ground is placed on the back side of the substrate [8,9]. At resonance frequency, the reflected wave is reduced due to the impedance matching between the material and air. Also, the transmitted wave is absorbed because of the loss of the absorber. However, the resonance-based MTM absorber has a narrow absorptivity bandwidth. To overcome this problem, dual-band MTM absorbers have been suggested by many researchers. For unit cell designs, some previous works have adopted asymmetric structures to generate additional resonance [10–13].

In this article, a dual-band metamaterial microwave absorber (DMMA) using asymmetric triangle split-ring resonators (TSRRs)